Journal of Zhejiang University-SCIENCE B (Biomedicine & Biotechnology)
ISSN 1673-1581 (Print); ISSN 1862-1783 (Online)
www.jzus.zju.edu.cn; www.springerlink.com
E-mail: jzus@zju.edu.cn

Integrated 3D bioprinting-based geometry-control strategy for fabricating corneal substitutes*

Bin ZHANG[1,2], Qian XUE[1,2], Han-yi HU[3], Meng-fei YU[4], Lei GAO[1,2], Yi-chen LUO[1,2], Yang LI[1,2], Jin-tao LI[1,2], Liang MA[†‡1,2], Yu-feng YAO[3], Hua-yong YANG[1,2]

[1]*State Key Laboratory of Fluid Power & Mechatronic Systems, Zhejiang University, Hangzhou 310058, China*

[2]*School of Mechanical Engineering, Zhejiang University, Hangzhou 310058, China*

[3]*Department of Ophthalmology, Sir Run Run Shaw Hospital, School of Medicine, Zhejiang University, Hangzhou 310016, China*

[4]*The Affiliated Stomatologic Hospital, School of Medicine, Zhejiang University, Hangzhou 310003, China*

[†]E-mail: liangma@zju.edu.cn

Received Apr. 9, 2019; Revision accepted Aug. 1, 2019; Crosschecked Oct. 11, 2019

Abstract: Background: The shortage of donor corneas is a severe global issue, and hence the development of corneal alternatives is imperative and urgent. Although attempts to produce artificial cornea substitutes by tissue engineering have made some positive progress, many problems remain that hamper their clinical application worldwide. For example, the curvature of tissue-engineered cornea substitutes cannot be designed to fit the bulbus oculi of patients. Objective: To overcome these limitations, in this paper, we present a novel integrated three-dimensional (3D) bioprinting-based cornea substitute fabrication strategy to realize design, customized fabrication, and evaluation of multi-layer hollow structures with complicated surfaces. Methods: The key rationale for this method is to combine digital light processing (DLP) and extrusion bioprinting into an integrated 3D cornea bioprinting system. A designable and personalized corneal substitute was designed based on mathematical modelling and a computer tomography scan of a natural cornea. The printed corneal substitute was evaluated based on biomechanical analysis, weight, structural integrity, and fit. Results: The results revealed that the fabrication of high water content and highly transparent curved films with geometric features designed according to the natural human cornea can be achieved using a rapid, simple, and low-cost manufacturing process with a high repetition rate and quality. Conclusions: This study demonstrated the feasibility of customized design, analysis, and fabrication of a corneal substitute. The programmability of this method opens up the possibility of producing substitutes for other cornea-like shell structures with different scale and geometry features, such as the glomerulus, atrium, and oophoron.

Key words: 3D bioprinting; Corneal alternative; Digital light processing (DLP); Extrusion; Geometry-control
https://doi.org/10.1631/jzus.B1900190 **CLC number:** R779.65; Q819

1 Introduction

Corneal diseases are one of the main causes of blindness. A severe shortage of donor corneas for clinical use, especially in developing countries, has resulted in about 10 million untreated patients on waiting lists for transplants, but fewer than 200 000 corneal transplantations have been performed each year (Gain et al., 2016). Therefore, research and development of artificial corneal substitutes is urgently needed.

‡ Corresponding author

* Project supported by the National Natural Science Foundation of China (Nos. 51875518 and 51475419), the Key Research and Development Projects of Zhejiang Province (Nos. 2017C01054 and 2018C03062), and the Fundamental Research Funds for the Central Universities (No. 2019FZA4002), China

ORCID: Liang MA, https://orcid.org/0000-0002-6242-1850

To alleviate the need for donor corneas, many research teams around the world have attempted to develop cornea substitutes. For example, decellularized porcine corneal stroma is treated as a cornea substitute after decellularization and antigen removal (Yoeruek et al., 2012), but immune rejection still occurs because of antibodies produced by humans to the residual cells in decellularized porcine matrices (Sasaki et al., 2009). Some studies using other natural or biosynthetic materials, such as amniotic membranes (Mi et al., 2010), hydrogels (Alaminos et al., 2006; Levis et al., 2012), silk fibroin (Lawrence et al., 2009, 2012), and recombinant collagen (Fagerholm et al., 2014) have been reported. However, such processes are often complicated and require manual effort, causing difficulties for fabrication. Furthermore, a lack of manufacturing repeatability and process stability makes conventional tissue engineering inconvenient for volume production and modification. A three-dimensional (3D) bioprinted cornea-like structure method reported by Isaacson et al. (2018) provided a proof-of-concept for the fabrication of cornea-like structures with a 3D printer, but the method cannot simulate the structural parameters and scale of a natural cornea. The prototype 3D model has low manufacturing accuracy and is larger than the natural human cornea, which limits the application and development of this method. These methods have not been widely promoted due to the limitations of the technology, since the structure of the membrane is usually uncontrollable in conventional tissue engineering. In addition to focusing on the transparency of the cornea, attention should also be given to the optical properties (Wang et al., 2018). The ideal cornea substitute would be a multi-layer structure with customizable geometrical characteristics based on individual eyeballs (Fig. 1). So, is it possible to construct cornea substitutes with specific geometric features?

Here, we propose a novel idea to combine digital light processing (DLP) and 3D extrusion printing to control the curvature and thickness of hollow structures with curved surfaces. An integrated 3D printer with DLP and extrusion printing modules was designed and fabricated. The hollow portion of the structure is constructed using the DLP module, while

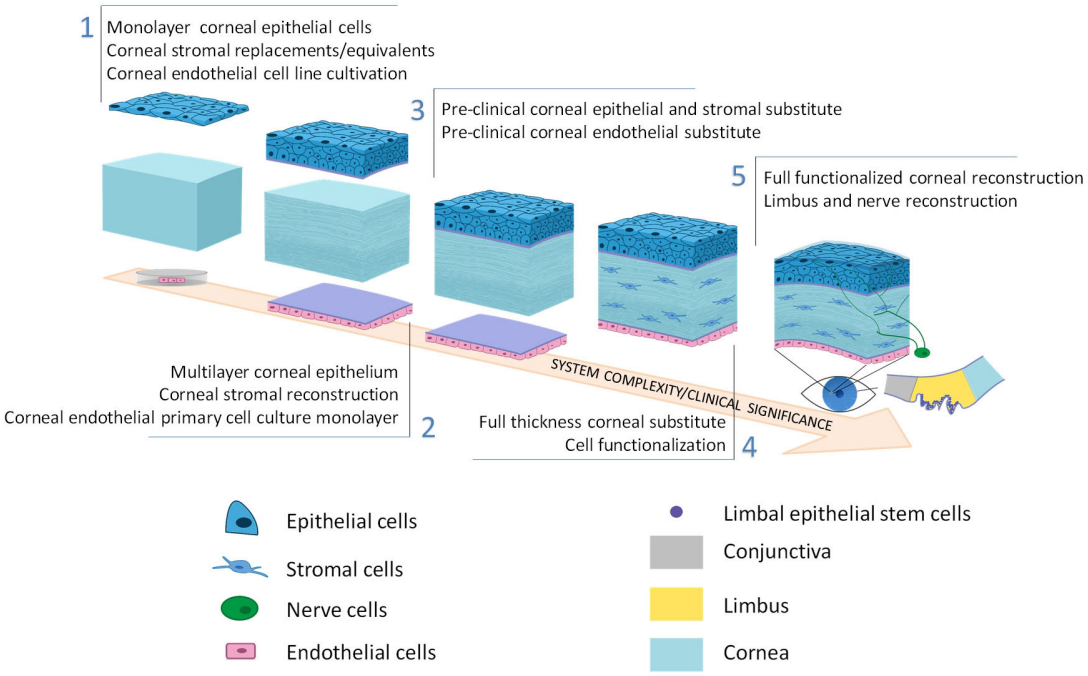

Fig. 1 Schematic of corneal substitute development

A full-thickness structure with both optical and biological properties is the aim of cornea substitute development. Reprinted from Zhang et al. (2019), Copyright 2019, with permission from Elsevier

the outer shell portion of the structure with a certain thickness is constructed using the extrusion printing module. Accurate geometric characteristic construction and multi-material combinations are the main advantages of 3D bioprinting technology (Ahadian and Khademhosseini, 2018). Using this method, it is feasible to manufacture geometry-controllable biosynthetic corneas with controllable thickness and curvature. The process of manufacturing 3D-bioprinted corneal scaffolds described in this article has potential applications not only for the study of corneal regeneration, but also for the fabrication of substitutes for other tissues and organs needing complex curved surface reconstruction.

2 Materials and methods

All the reagents used were purchased from Aladdin Reagent Co. (Shanghai, China) except when otherwise specified.

2.1 Preparation of sodium alginate-gelatin solution for extrusion printing

Sodium alginate used was of analytical reagent grade and medium viscosity pharmaceutical grade, and the analytical-reagent-grade gelatin was alkali-processed type B material. Sodium alginate powder and gelatin powder (Sigma-Aldrich, Shanghai, China) and calcium chloride ($CaCl_2$) powder were sterilized under ultraviolet (UV) light for 30 min. Films were prepared by blending 0.02 g/mL sodium alginate and 0.10 g/mL gelatin aqueous solutions. First, gelatin was dissolved in deionized water at 50 °C to a concentration of 0.10 g/mL, followed by stirring until the solute was dissolved completely. Then 0.02 g/mL sodium alginate was dissolved in the solution by hydration and the mixture was stirred for 2 h at 400 r/min. The homogenous mixture was dispensed and sealed in centrifuge tubes at 4 °C. $CaCl_2$ solution (0.05 g/mL) was prepared for use.

Four acellular bioinks with different concentrations of alginate-gelatin were prepared for optimal thickness control according to our previous work on the extrusion printing process (Zhang et al., 2017): (1) S-1: 0% sodium alginate and 0.10 g/mL gelatin aqueous solutions; (2) S-2: 0.01 g/mL sodium alginate and 0.10 g/mL gelatin aqueous solutions; (3) S-3: 0.02 g/mL sodium alginate and 0.10 g/mL gelatin aqueous solutions; (4) S-4: 0.04 g/mL sodium alginate and 0.10 g/mL gelatin aqueous solutions.

Human corneal epithelial cell (HCEC) line was used to test the effect of manufacturing methods on cell viability. HCECs were cultured in Dulbecco's modified Eagle medium/nutrient mixture F-12 (DMEM/F12; Gibico, Carlsbad, CA, USA) supplemented with 5% fetal bovine serum (FBS), human recombinant insulin (5 mg/mL, Sigma), and epidermal growth factor (EGF; 10 μg/mL, Abbkine). Cells were incubated in polystyrene tissue culture flasks at 37 °C in 5% CO_2, fed with fresh medium every other day, and passaged every 4 d.

HCECs were used to prepare the cell-laden bioink. After washed with phosphate-buffered saline (PBS), cells were exposed to trypsin-ethylene diamine tetraacetic acid (EDTA) solution (0.25%:0.02%) for 5 min at 37 °C in 5% CO_2, followed by centrifugation at 1000 r/min for 5 min. Then the cells were resuspended in the sodium alginate-gelatin solution to a concentration of 2×10^6 cells/mL. The cell suspension was mixed gradually and slightly with pipette to prevent bubbles.

2.2 Preparation of gelatin methacryloyl solution for DLP printing

We identified an ideal material for high-fidelity bioprinting based on multifaceted comparisons and the work of Ying et al. (2018). Gelatin methacryloyl (GelMA) hydrogel was synthesized according to the method of Bae et al. (2011) and Gill et al. (2018). Briefly, 4 g gelatin was mixed with 40 mL PBS solution. The solution was stirred and heated to 50 °C until the gelatin was fully dissolved. While maintaining the temperature, 3 mL methacrylate was added to the solution at a rate of 0.3 mL/min, and the solution was controlled between pH 8 and pH 9 by adding 10 g/mL NaOH solution. Stable conditions were maintained to allow reaction for 90 min. After stopping the reaction by adding 200 mL PBS, the mixture was then dialyzed against distilled water using 10–13 kDa dialysis tubing for one week, while changing the distilled water every 12 h. Finally, the solution was lyophilized to remove water and the obtained white spumescent GelMA was stored at 4 °C. In the DLP printing process, a conventional commercial DLP printer was used to print the hollow part as substrate. The concentration of

GelMA was 0.15 g/mL as bioink, and the substitution of methacrylate was 0.65 g/mL. The power of the light source was 40 mW/cm^2 (wavelength 405 nm).

2.3 Data acquisition and 3D modelling

The cornea can be divided into four zones: the central, paracentral, peripheral, and limbal zones (Fig. 2). The whole cornea is nearly toric surface, while the central zone is almost spherical (Burek and Douthwaite, 1993). The central zone is also known as the functional optical zone, which plays the role of refracting light. The thickness and curvature in the central zone are almost consistent. The cornea is a meniscus lens that, in conjunction with the anterior chamber, forms a compound convex lens. As the interface between the air and the eye, the corneal anterior surface accounts for about 48 diopters (D) of the whole eye (Gullstrand, 1910; Kiely et al., 1982). A commercial medical scanning instrument, the Pentacam (HR Typ 70900, OCULUS, Germany) was used for primary data measurement of a natural human cornea. A mathematical model was used to simulate and estimate the parameters affecting the cornea. This model was applied to analyze the factors influencing the corneal refractive power and to explore methods for controlling them. Therefore, the key parameters affecting corneal optical function were determined and structures related to these parameters were designed and modelled.

2.4 Fabrication of cornea substitutes

The method for fabricating cornea substitutes is shown in Fig. 3.

2.4.1 Fabrication of the hollow portion as the printing substrate

Based on data obtained with the Pentacam, computer-aided design was used to construct a 3D printing model consistent with the posterior corneal surface curvature topography. The average of the scanning results of natural human corneas (8 mm) was set to be the curvature radius of the printed substrate. The hollow portion of the corneal scaffold (Fig. 3) was prepared by DLP-based bioprinting, using the method reported by Na et al. (2018). The dynamic optical projection stereolithography (DOPsL) platform of the DLP printer consists of millions of micromirrors which solidify the photopolymer solution by regulating the UV light into different optical patterns and lifting the stage with the printed object. The topography and pattern of the substrate were constructed well and fast owing to the superior printing speed and resolution of the DLP.

2.4.2 Fabrication of curved calcium alginate-gelatin films with extrusion printing

The film as a corneal substitute was fabricated using an extrusion printing module on the printing substrate (Fig. 3). We generated the G-code according to the concentric-circle printing trajectory and imported the program into the control system of the extrusion-based 3D bioprinter. Bioink was loaded into a syringe mixing system, free of air bubbles by an ultrasonicator connected to the extrusion nozzle (Fig. 3). In this process, the blending solution was extruded from the injector (the size of nozzle: 0.25 mm)

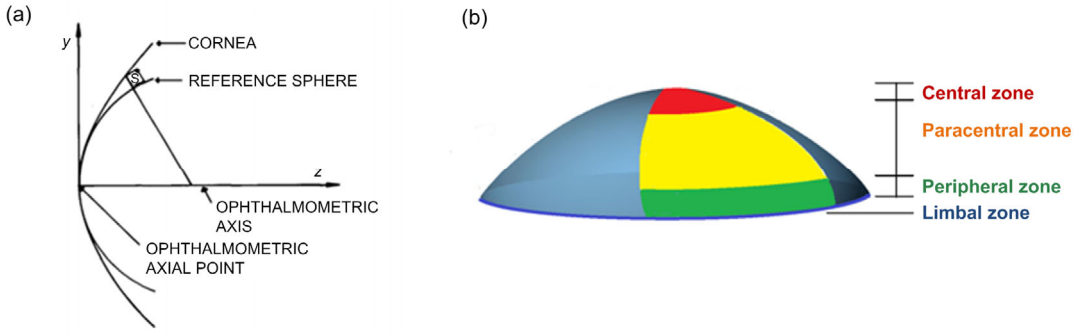

Fig. 2 Structure of cornea

(a) A cross-section schematic of the human cornea and a reference sphere, which are approximately coincident in the central zone. Reprinted from Kiely et al. (1982) by permission of Taylor & Francis Ltd. (b) Four zones of the cornea

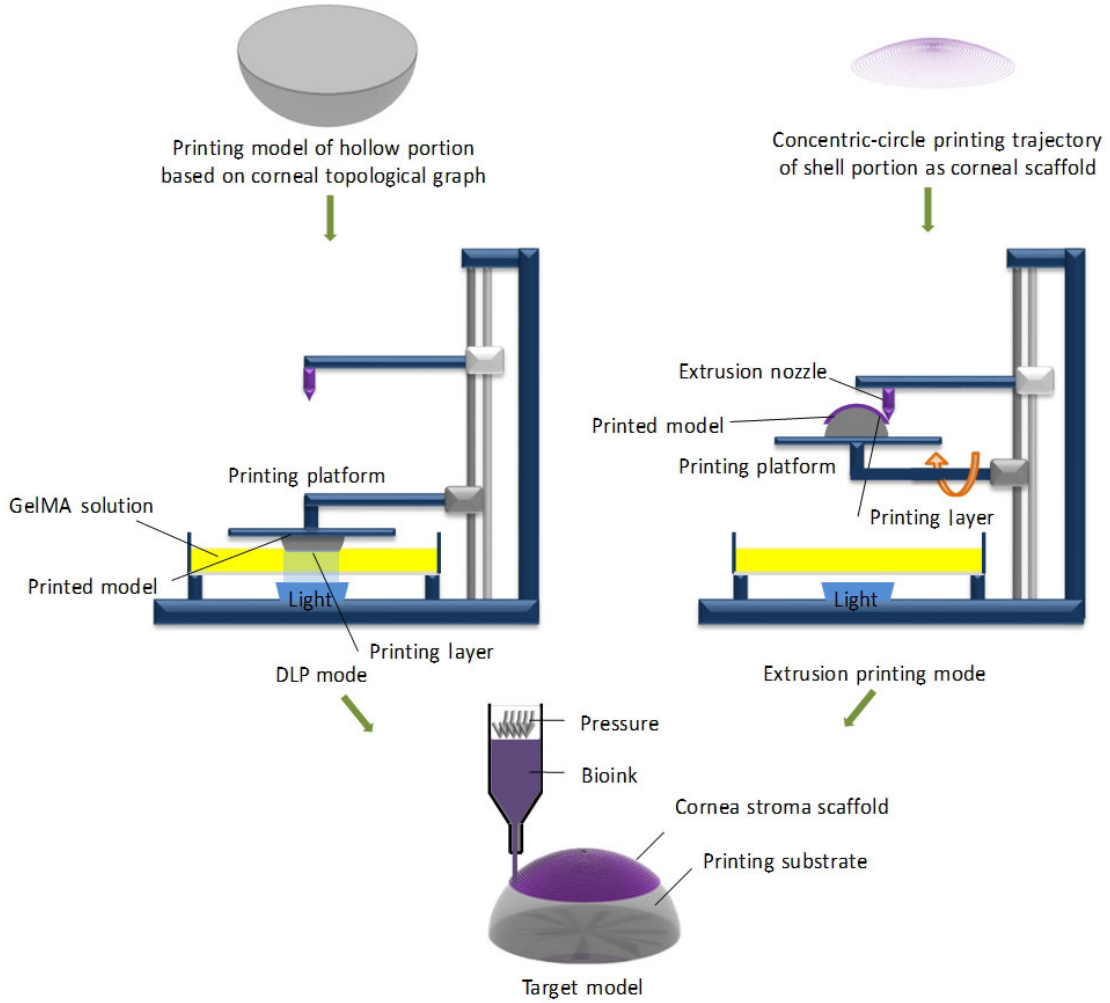

Fig. 3 Schematic of the combined 3D bioprinting method for a corneal scaffold
GelMA, gelatin methacryloyl; DLP, digital light processing

and printed on the GelMA substrate according to preset printing parameters and debugged motion track. The thickness of the corneal substitute was controlled by changing the extrusion pressure during the printing process. Films were then sprayed with $CaCl_2$ solution to solidify the bioink solution into hydrogel. The unreacted Ca^{2+} on the surface of the corneal scaffold was removed by washing three times with PBS. The printed corneal scaffold was transferred into a petri dish filled with isotonic solution to maintain the equilibrated hydrated state, and stored at 4 °C. The samples were printed with an optimum proportion of sodium alginate at air pressures under 0.50, 0.55, 0.60, 0.65, 0.70, 0.75, and 0.80 bar (1 bar=100 kPa), separately, based on our previous work (Zhang et al., 2017).

2.5 Evaluation of printed films

2.5.1 Surface roughness

The morphology and surface topography of the corneal scaffold were observed using a light microscope (Olympus, Beijing, China) and a scanning electron microscope (SEM; JEM-6700F, JEOL Co., Ltd., Tokyo, Japan). For SEM images, the films were dried and cut into smaller specimens (2 mm×2 mm) attached to carbon tape. Then the specimens were sputter-coated with a thin layer of electrically conducting material on the surface. Micrographs of the coated specimens were taken under vacuum conditions. All the specimens were lyophilized before measurement.

2.5.2 Curvature and thickness

To reduce the sensation of grittiness and foreign body sensation after implantation caused by the corneal scaffold, and to achieve refractive function through the difference in thickness of the edge and center, as well as to achieve a good fit in the corneal bed, it was necessary to measure the curvature and thickness of the printed corneal scaffold. The curvature radius of the DLP-printed corneal substrate was measured with an optical surface metrology device used to scan and reconstruct the printed substrate. The thickness needs to be measured in an equilibrated hydrated state without any deformation or damage. Therefore, the thickness of the scaffolds was measured using a scanning acoustic microscope system, which supports multi-layer scanning imaging and nondestructive testing of material structural parameters. The horizontal resolution was 2.5 μm and the vertical resolution 5 μm, while the maximum penetration depth was 10 mm, which met the design requirements. The samples printed with S-3 were measured to explore the effect of printing parameters on the thickness of the film. The samples were placed in a beaker containing pure glycerin with their concave face down. The vertical-section thickness of each sample was taken from the average of three or more measurements.

2.5.3 Mechanical properties

The stromal layer is the main component of the cornea, accounting for about 90% of the total thickness. Therefore, good mechanical performance of the printed corneal scaffold is required, including elasticity characteristics to withstand the intraocular pressure. Stress-strain measurements were carried out using a uniaxial loading with a range of 20 N and a crosshead speed of 0.5 mm/min at room temperature delivered by an Electro Force Universal Testing Machine (TA Instruments, New Castle DE, USA). The tensile strength and elastic modulus of the samples were determined by computing the maximum stress. To monitor the response of the film printed with S-3 at an air pressure of 0.50 bar, samples in an equilibrated hydrated state were designed to be dumb-bell shaped specimens with uniform cross section (width 2 mm, thickness 5 mm, guage length 10 mm, and a 10-mm area on both sides for gripping) and examined at an initial grip separation of 10 mm.

2.5.4 Transmittance

In most studies, the transparency of artificial corneal equivalents was evaluated by placing them above the pattern, and subjectively evaluating the degree of transparency by comparing differences in clarity. Evaluating the degree of transparency objectively can be achieved by calculating the percentage of luminous flux before and after passing through the specimen. Therefore, we developed a method to quantitatively measure the transmittance of printed film. According to the Beer-Lambert law, the transmittance is related to optical depth and absorbance by (in the case of uniform attenuation)

$$T=\mathrm{e}^{-\alpha\tau}=10^{-A}, \tag{1}$$

where T is the transmittance, τ is the optical depth, A is the absorbance, and α is the attenuation coefficient (the coefficient is related to the density and concentration of the bioink). The bioink was divided into 96-well plates with different volumes. The absorbance of bioink at different depths in the 300–700 nm bands was measured using a spectrophotometer, thereby fitting the relationship between α and depth. According to this relationship, we could calculate the specific transmittance of printed samples of different thicknesses. This method is simple, effective, and accurate.

2.5.5 Water content and the degree of swelling

The water content of the corneal scaffold was characterized by wet-to-dry weight ratios. The mass of the printed corneal scaffold in an equilibrated hydrated state (m_{hydrated}) and a dry state (m_{dry}) was tested. The water content was defined as

$$(m_{\mathrm{hydrated}}-m_{\mathrm{dry}})/m_{\mathrm{hydrated}}\times 100\%. \tag{2}$$

Deionized water on the surface of the film was adsorbed with clean paper, and the weight of film in the equilibrated hydrated state was measured using an analytical balance (ME54T/02, METTLER TOLEDO; Zurich, Switzerland), while the dry weight of the film was measured after lyophilization.

Pre-weighed printed corneal scaffolds were immersed in distilled water for 24 h. The mass of samples in a swelling state was measured. Measurements were carried out until the weight of the swollen films

($m_{swollen}$) attained a constant value. The degree of swelling was calculated by

$$(m_{swollen}-m_{hydrated})/m_{hydrated}\times 100\%. \quad (3)$$

3 Results

3.1 Mathematic modelling and customized scaffold design

Laser refractive surgery (LRS) on the cornea modifies the anterior corneal curvature by ablation of corneal tissue. DLP-extrusion-bioprinted corneal substitute implantation is the reverse operation of LRS to correct refractive error. To reduce the refractive power of the cornea, the corneal scaffold is designed to be a negative meniscus lens (Fig. 4a) (if designed to increase refractive power, the corneal scaffold would be designed as a positive meniscus lens; here we consider only the former case). According to the mathematical model, key parameters affecting the optical capacity of the corneal substitute can be analyzed by calculation.

For simplicity, we viewed the central zone of the cornea as a simple first-order Gaussian optics surface. Other relevant aspects, such as intracorneal scattering, were considered negligible. The key geometric parameters of the corneal substitute that affect its refractive ability were calculated with the mathematic model. The model was thus described by a single variable, the corneal anterior surface curvature R. The posterior surface curvature of the corneal scaffold was designed to be the same as the curvature of the spherical surface of the corneal central zone, so as to achieve a better fit between the corneal scaffold and the corneal graft bed. Light will refract at the anterior boundary of the corneal scaffold and move to the posterior boundary where it will refract again.

The imagining principle of a concave lens (Fig. 4c) is equal to a combination of a plane convex lens and a plane concave lens. Taking a plane convex lens into consideration, according to the theory of basic optics,

$$f_1=R_a/(n-1), \quad (4)$$
$$f_2=R_p/(n-1). \quad (5)$$

According to the Gaussian optics formula, the focal length of the lens can theoretically be inferred from the mathematical model of a negative meniscus lens, where f is the focal length of the cornea scaffold (f_1: anterior surface; f_2: posterior surface), R_a is the anterior surface curvature, R_p is the posterior surface curvature, and n is the refractive index of the cornea scaffold:

$$f=\frac{f_1 f_2}{f_1+f_2}=\frac{R_a R_p}{(n-1)(R_a+R_p)}. \quad (6)$$

According to the geometrical theorem, the geometrical relationship between the variables is as follows:

$$T_c+R_p+L=R_a, \quad (7)$$
$$\sqrt{R_a^2-(\phi/2)^2}-\sqrt{R_p^2-(\phi/2)^2}-L=T_e, \quad (8)$$

where ϕ is the diameter, L is the center distance, T_c is the center thickness, and T_e is the edge thickness.

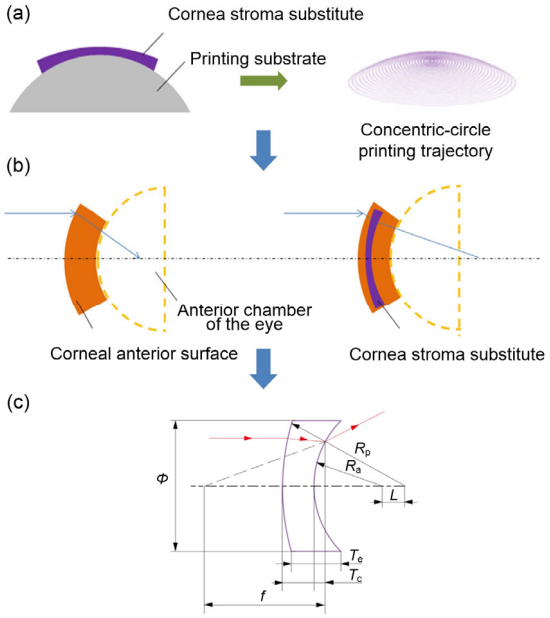

Fig. 4 Analysis of key geometry parameters of cornea and cornea stroma substitute

(a) Print strategy diagram and the concentric-circle motion trajectory of the extrusion nozzle based on a cornea thickness topological graph, assisted by a computer-aided design program. (b) Light path diagram of the cornea before and after the corneal scaffold implantation. (c) The mathematical model of refraction in a corneal scaffold as a negative meniscus lens. ϕ, diameter; R_a, anterior surface curvature; R_p, posterior surface curvature; L, center distance; T_e, edge thickness; T_c, center thickness; f, focal length of the cornea scaffold

We conclude that when the value of R_p is a constant, increasing the thickness difference of the negative meniscus and cutting or reducing the thickness of the center thickness can contribute to an increase in the refractive power of the corneal scaffold, when the posterior surface curvature of the corneal scaffold and the refractive index of the material are constants. Therefore, the controllable thickness of the corneal substitute is a key research goal, and the curvature of the posterior surface is the key factor to ensure the adaptability of corneal replacement.

We modelled the 3D target geometry (Fig. 5), including a cornea height topological graph, cornea curvature topological graph, and cornea thickness topological graph, based on human corneal surface data obtained from natural corneas using the Pentacam. A standard stereolithography file format (.stl) was constructed as a pre-scaffold for corneal reconstruction with the 3D target data. The motion trajectory of the extrusion nozzle was set as a concentric circle centered on the focus of the cornea, similar to that of a natural cornea (Fig. 5e).

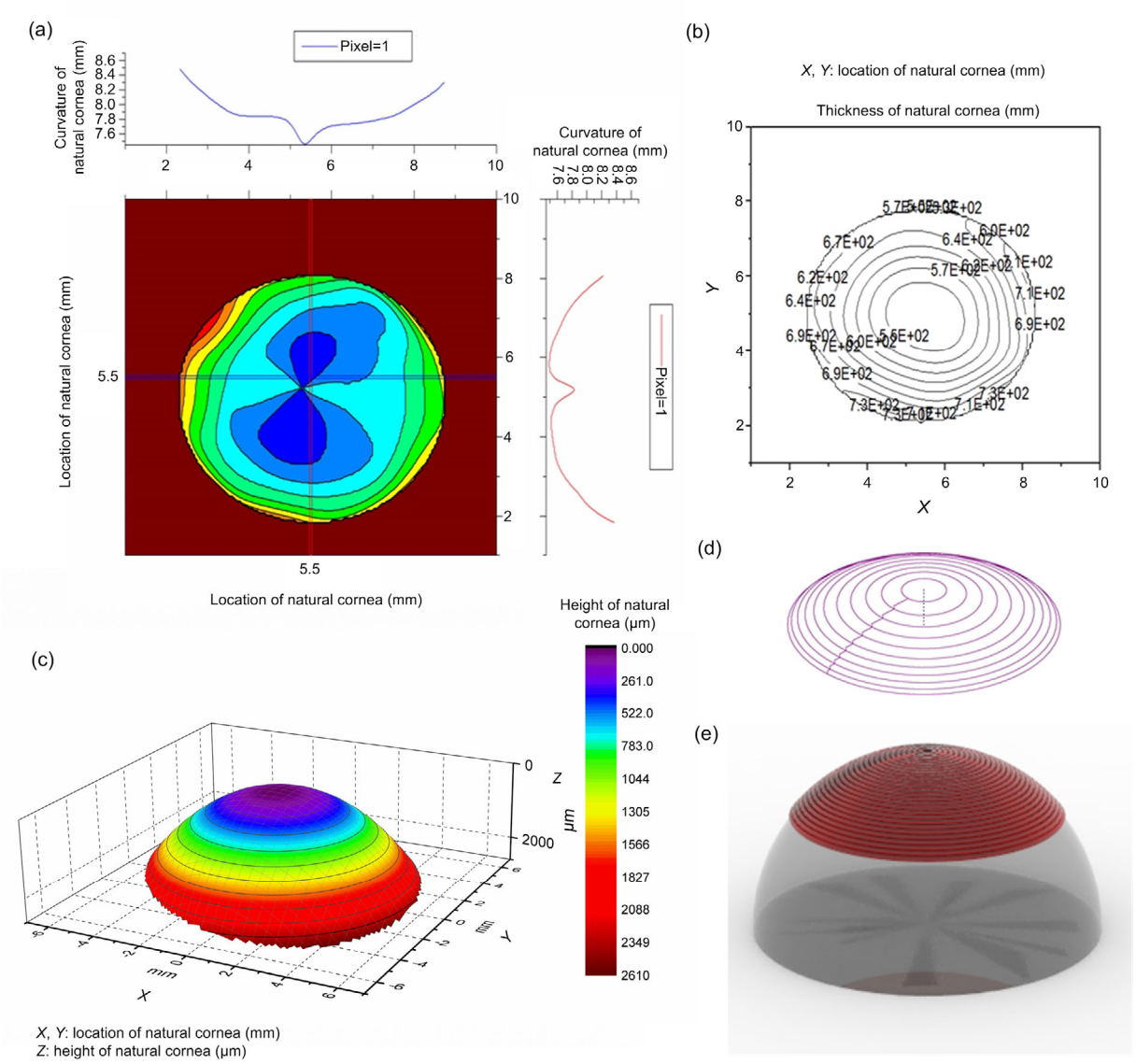

Fig. 5 3D target geometry model of cornea

(a) Cornea curvature topological graph; (b) Isopach distribution of thickness; (c) Cornea height topological graph; (d) Motion trajectory of the extrusion nozzle set as a concentric circle; (e) Computer simulation model of the substrate and printed corneal substitution

3.2 Surface characterization and transparency

The micrographs show that the different properties of the bioinks resulted in tremendous diversity in printability. The performance of the film printed with S-3 bioink was better than that of S-2 or S-4. The film printed with S-3 was more integrated, compact and uniform, with a smoother surface and better structural formability. In the dry state (Fig. 6e), the film printed with S-3 presented excellent surface accuracy and roughness. These films printed with the optimal bioink showed good transparency, making them suitable candidates for use as corneal scaffolds (Fig. 6). To visualize the transparent films, moderate amounts of orchil were added to the bioink.

3.3 Measurement of curvature and thickness

The hollow part of the curved structure was constructed with DLP as the substrate for extrusion printing (Fig. 7a). The gray area in Fig. 7b marks the area used for curvature measurement. The curvature of the printed substrate was calculated to be 7.915 mm, which is similar to the design print model radius (8 mm). When the air pressure was 0.5 bar, the average center thickness of the printed film was 180 μm (Fig. 7c). The extrusion pressure was approximately linear. According to the measurement results, the central thickness of the film reduced with decreasing pressure. A film with a center thickness of 200–600 μm could be printed by adjusting the extrusion pressure, with a thickness manufacturing accuracy of less than 100 μm (Fig. 7d).

3.4 Measurement of the transmittance of the printed corneal substitutes

The absorbance of different bioinks in the 300–700 nm bands was measured with a spectrophotometer. The relationship between the attenuation coefficient α and the thickness of different bioinks was fitted according to the Beer-Lambert law (Fig. 8a).

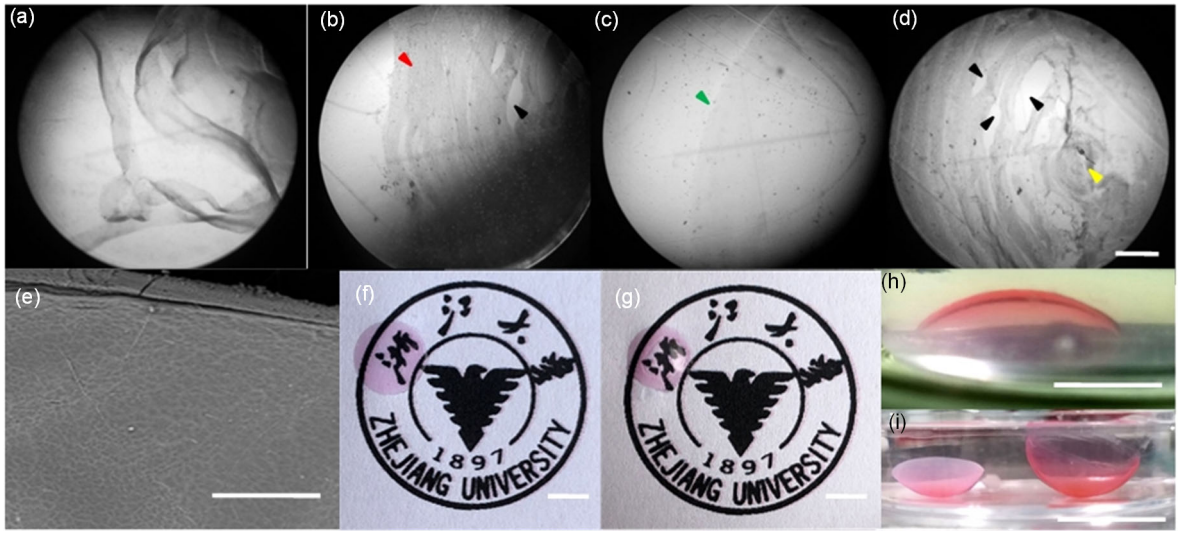

Fig. 6 Printed curved corneal scaffold utilizing bioinks with different concentrations

Micrographs of films with different bioinks (S-1, S-2, S-3, S-4), made with the same printing process at room temperature (scale bar=500 μm): (a) printed S-1 film was in a semi-solid state and easily unraveled at room temperature and the structure could not be formed; (b) due to the fluidity of the bioink, the film structure printed with S-2 was deposited from the centre to the edge (red arrow), and there were some gaps (black arrow) in the structure because of the bad combination of the bioink filament; (c) the edge and surface (green arrow) of the film printed with S-3 was smooth and integrated, and there was no obvious pattern in the structure; (d) the formability of printed S-4 film was poor, and the bioink filaments intertwined and became entangled with each other in the final stage of the printing process, resulting in uneven distribution of bioink (yellow arrow). (e) Scanning electron microscope (SEM) image of the top surface of a printed film (scale bar=200 μm). (f) Printed flat film with good transparency (scale bar=5 mm). (g) Printed curved film with good transparency (scale bar=5 mm). (h, i) Examples of 3D printed calcium alginate-gelatin film with S-3 in an equilibrated hydrated state (scale bar=5 mm (h) and 10 mm (i), respectively) (Note: for interpretation of the references to color in this figure legend, the reader is referred to the web version of this article)

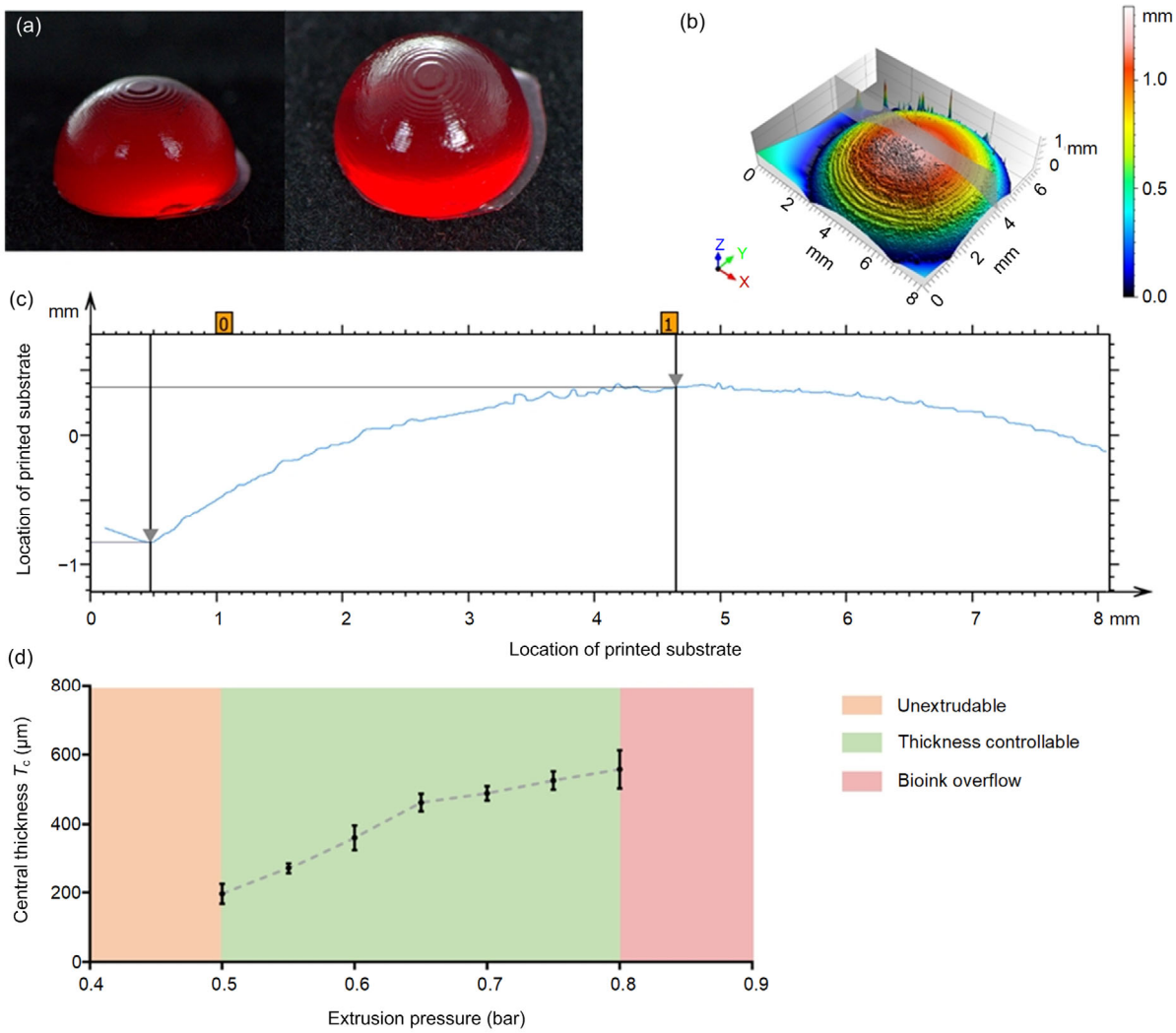

Fig. 7 Controlling process of key parameters

(a) Digital light processing (DLP)-printed hollow portion as a printed substrate of a corneal substitute (gelatin methacryloyl mixed with red dye). (b) The 3D surface metrology of a DLP-printed corneal substrate and the scanning area of curvature measurement (gray area). (c) The geometry data of the cross-sectional view in the DLP-printed corneal substrate. The vertical height was 1.2 mm, and the horizontal radius 4.19 mm. The radius of the DLP-printed corneal substrate was calculated to be 7.915 mm, which is close to the radius of the designed model for DLP (8 mm). (d) Central thickness-pressure relationship line chart (the samples were printed with S-3 at air pressures of 0.50, 0.55, 0.60, 0.65, 0.70, 0.75, and 0.80 bar (1 bar=100 kPa)). The data are expressed as mean±standard deviation (n=6)

The attenuation coefficient α was very consistent with the thickness relationship in the same bioink. This fitting relationship can be used effectively to calculate the transmittance of a specimen with different thicknesses. Based on the fitting relationship, we calculated the transmittance of the printed sample. The average transmittance of films printed with S-3 bioink was 85%–94% in the visible spectrum (Fig. 8b). In the ultraviolet and blue-violet bands, the printed film had a low transmittance, giving it the potential to avoid radiation damage to the tissue.

3.5 Evaluation of mechanical properties

The dependence of tensile strength and breaking elongation on the content of sodium alginate in the bioink is shown in Fig. 8c. The percentage of sodium

alginate had a significant impact on the mechanical properties of the bioinks. S-2, S-3, and S-4 showed a uniform incremental Young's modulus. The maximum value that appeared at 0.04 g/mL sodium alginate content reached 0.2 MPa, much higher than those of the other two bioinks. All the bioinks exhibited an approximately linear behavior. Multiple factors may contribute to the elongation increasing to breakage point, such as the effects of plasticization, or ion interaction between sodium alginate and gelatin. In the tensile stress measurement, the S-1 bioink could not form a stable structure at 32 °C, so the experiment using S-1 was omitted (Figs. 8c and 8d).

3.6 Water content characterization

The degree of swelling of the blended films decreased with increasing sodium alginate content, while there was a small difference in the water content. Using S-3 bioink, the average rate of swelling of the printed film was 15%, and the water content was 89%. This result may be attributed to various factors. In the printed films with a high sodium alginate concentration, the ability of the gelatin polymer network to physically entangle the alginate molecular chain is limited. During the soaking and swelling process, excess alginate diffuses into the solution, resulting in a negative swelling rate. The rate of permeation of molecules through the polymer network structure depends predominantly on the swelling ability of the network in the medium of transport. The water content of the cornea is closely related to its visible wavelength transparency, refractive capabilities, and penetration capacity. The water content of the film printed by S-3 material (Fig. 8e) was close to that of the natural cornea. A lower swelling ratio can avoid deformation of the printed structure.

3.7 Cell viability

The HCECs in the printed corneal scaffolds retained greater than 80% viability (Fig. 9). The 3D live/dead stain images demonstrated that the HCECs were distributed uniformly in the printed film. The curved geometric characteristics of cells in the printed corneal scaffolds were clear and smooth, showing that this manufacturing method had caused little damage to cells, and supports cell-containing manufacture.

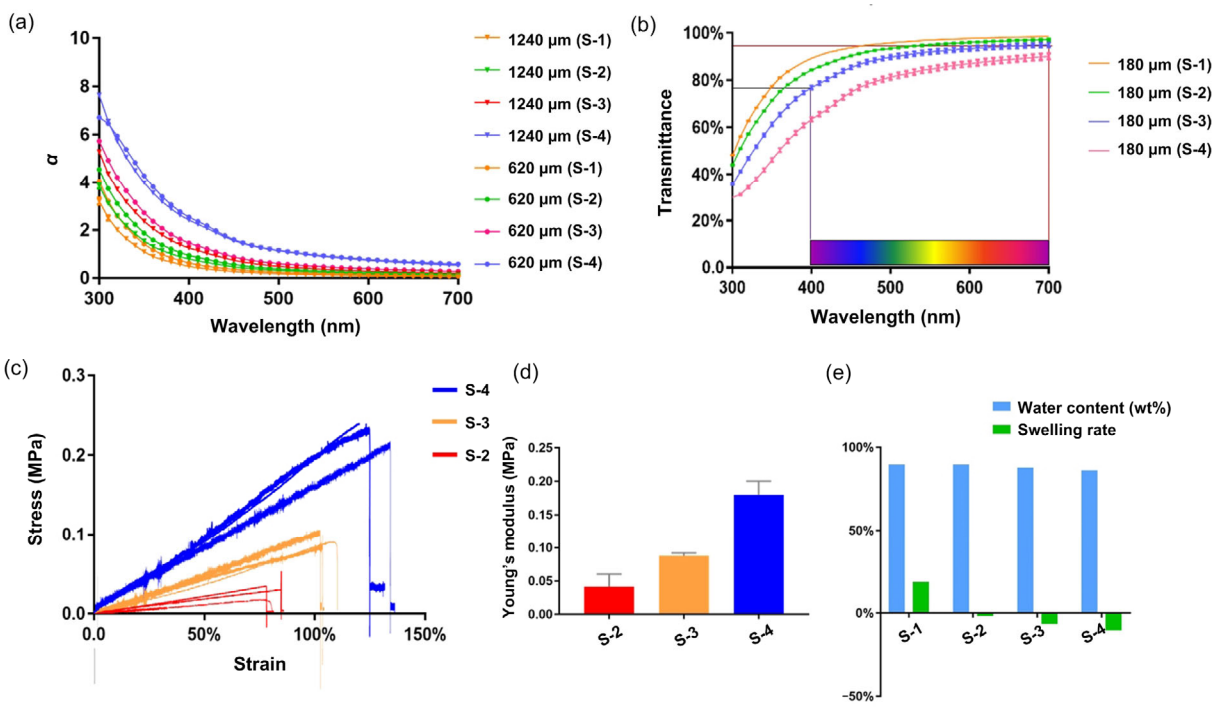

Fig. 8 Evaluation of printed corneal scaffold

(a) The relationship between the attenuation coefficient α and the thickness (620 and 1240 μm) of different bioinks. (b) Transmittance of a printed corneal scaffold with a central thickness of 180 μm. (c) Stress–strain curves of S-2, S-3, and S-4. (d) Young's modulus of S-2, S-3, and S-4. (e) The degree of swelling and water content (w/w) of the bioinks. The data (b, d) are expressed as mean±standard deviation (n=3)

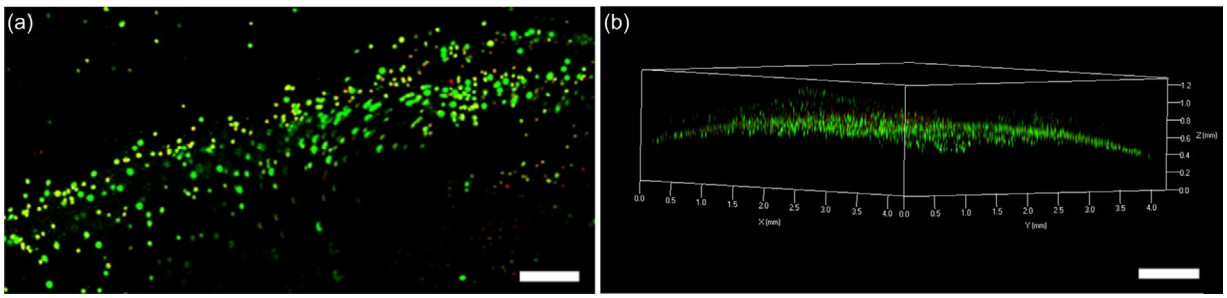

Fig. 9 Cell viability of printed corneal scaffold

(a) Representative live/dead stained confocal image of printed HCEC-laden microfibrous tissue (scale bar=500 μm); (b) Representative 3D live/dead stained confocal image of printed HCEC-laden film (scale bar=1000 μm)

4 Discussion

Improved fabrication strategies for artificial corneal substitutes, or even corneal equivalents, are under intense investigation, in an effort to overcome the limitations of current methods. Some researchers have proposed novel techniques for fabricating human corneal substitutes. For example, Alaminos et al. (2006) fabricated a cornea equivalent using cultured keratocytes and an air-liquid culture technique. Kim et al. (2019) introduced a cornea-derived decellularized extracellular matrix (Co-dECM) as a 3D bioink to print flat film as a corneal substitute. These processes can support only the manufacture of flat membranes or geometry-uncontrollable cornea-like surfaces. When a flat membrane is used as a graft, the deformation of the material itself may cause mechanical stimulation of the recipient tissue leading to inflammation (Torricelli and Wilson, 2014). The introduction of 3D printing in the biomedical field is a relatively new attempt to reconstruct structures and functions that are difficult to achieve with conventional manufacturing methods. 3D printing can be an effective approach for fabricating cornea substitutes with complex geometry. Isaacson et al. (2018) applied a 3D printing method to construct a cornea-like curved structure. They printed with sodium alginate and methacrylated type I collagen on a 3D-printed plastic support structure. However, the geometric scale of the printed structure was much larger than that of a natural cornea, and the surface quality was not ideal. Duarte Campos et al. (2019) described a bioprinted corneal substitute made with collagen-based bioinks and primary human keratocytes. The printing of a full construct with a 20-mm diameter and 0.3-mm thickness took about 1 h. Therefore, the suitability of their application as a corneal implant is questionable. Compared to these products, the custom-designed corneal substitutes we propose avoid such problems as they can fit precisely on the recipient eye ball, with a size and surface smoothness suitable for cornea substitution along with a much faster fabrication process.

The integrated 3D bioprinting method we propose combining extrusion printing and DLP can significantly improve manufacturing accuracy. The hollow part of the curved corneal substitute is constructed by DLP printing. Data from the human eye were collected to build a model for printing and to ensure that the curvature of the printed film was similar to the geometry of a natural cornea. Thickness variation can be achieved by controlling the extrusion pressure. Our manufacturing process allows for high precision control and the construction of corneal substitutes that have the same size as a natural cornea or even thinner, which improves the clinical potential of 3D-bioprinted corneal substitutes. The entire manufacturing process takes less than 10 min with high quality and a high repetition rate, and is free of manual operation. It avoids the instability and low repeatability that can be caused by complicated manual operations in conventional fabrication processes. We experimented with four different ratios of bioinks and seven extrusion pressures based on our previous work (Zhang et al., 2017). The transparency of all the 3D-printed calcium alginate-gelatin films makes them a suitable candidate for corneal implants (Meek and Knupp, 2015). Moreover, the water content and degree of swelling of the printed film were similar to those of natural corneal stroma (78%) (Taylor et al.,

2015). Other materials can be used as printing bioinks according to needs, and drugs or factors can be printed into specific positions within the structure. The results demonstrate that a geometry-controllable film for artificial biosynthetic corneas can be prepared by 3D bioprinting and can overcome the limitations of current fabrication methods. Our study indicates that in future research 3D-bioprinted geometry-controllable film printed with this method has the potential to be used as a pre-substitute for reconstruction of corneas and other shell-like structures, as well as hollow structures with complex surfaces.

Isaacson et al. (2018) and Duarte Campos et al. (2019) have conducted a more detailed evaluation of printability with cell-laden ink. In our study, we focused more on manufacturing precision and geometry control. We hope to build a cell-free scaffold, which functions as a patch and will not cause cell-induced immune rejection. In addition, in our high-precision printing method, the loss of cells due to printing has been shown to be minimal, suggesting that our method could also be applied to the manufacture of cell-laden structures. The modification of bioinks and a series of in vivo animal experiments need to be carried out to explore the effects of the in vivo environment on the performance and properties of 3D-bioprinted corneal substitutes. Geometric control could be achieved more accurately by improving manufacturing equipment, printing processing and bioink in follow-up studies. With further optimization, we expect to develop an implantable, biocompatible, mechanically robust, effective and fully-functional corneal substitute to address the shortage of donor corneas and the defects of existing cornea alternatives.

5 Conclusions

We developed an integrated 3D bioprinting strategy for constructing geometry-controllable corneal substitutes, which combines the advantages of extrusion printing and DLP printing. Owing to its structural controllability and other advantages, the construction of a geometry-controllable artificial biosynthetic cornea has proved that this method could be a powerful tool for the fabrication of hollow structures with curved surfaces. Printed films could serve as a pre-scaffold for corneal regeneration and as replacements for donor corneas. Results suggest that the control and reconstruction of geometric characteristics can overcome the limitations of conventional manufacturing methods. The appropriate material and extrusion printing parameters were selected to realize the control of the thickness and curvature radius of the 3D-printed corneal substitute. A corneal scaffold of a similar scale and structure to the native cornea can be quickly constructed with this method. This research paves the way for further study of the in vitro construction of diopter-control corneal stromal substitutes and corneal reconstruction in vitro. Our results suggest that a customizable geometric structure and optical performance can be achieved. This method is a potential tool for the fabrication of corneal scaffolds with controllable geometric characteristics as an alternative to donor corneas.

Contributors

Bin ZHANG, Qian XUE, Liang MA, and Han-yi HU planned the study and performed the experimental work and data analysis. Qian XUE wrote the manuscript. Meng-fei YU, Lei GAO, Yi-chen LUO, Yang LI, Jin-tao LI, Yu-feng YAO, and Hua-yong YANG assist in reviewing papers. All authors read and approved the final manuscript. Therefore, all authors had full access to all the data in the study and take responsibility for the integrity and security of the data.

Compliance with ethics guidelines

Bin ZHANG, Qian XUE, Han-yi HU, Meng-fei YU, Lei GAO, Yi-chen LUO, Yang LI, Jin-tao LI, Liang MA, Yu-feng YAO, and Hua-yong YANG declare that they have no conflict of interest.

This article does not contain any studies with human or animal subjects performed by any of the authors.

References

Ahadian S, Khademhosseini A, 2018. A perspective on 3D bioprinting in tissue regeneration. *Bio-Des Manuf*, 1(3): 157-160. https://doi.org/10.1007/s42242-018-0020-3

Alaminos M, del Carmen Sánchez-Quevedo M, Muñoz-Ávila JI, et al., 2006. Construction of a complete rabbit cornea substitute using a fibrin-agarose scaffold. *Invest Ophthalmol Vis Sci*, 47(8):3311-3317. https://doi.org/10.1167/iovs.05-1647

Bae H, Ahari AF, Shin H, et al., 2011. Cell-laden microengineered pullulan methacrylate hydrogels promote cell proliferation and 3D cluster formation. *Soft Matter*, 7(5): 1903-1911. https://doi.org/10.1039/c0sm00697a

Burek H, Douthwaite WA, 1993. Mathematical models of the

general corneal surface. *Ophthalmic Physiol Opt*, 13(1): 68-72.
https://doi.org/10.1111/j.1475-1313.1993.tb00428.x

Duarte Campos DF, Rohde M, Ross M, et al., 2019. Corneal bioprinting utilizing collagen-based bioinks and primary human keratocytes. *J Biomed Mater Res Part A*, 107(9): 1945-1953.
https://doi.org/10.1002/jbm.a.36702

Fagerholm P, Lagali NS, Ong JA, et al., 2014. Stable corneal regeneration four years after implantation of a cell-free recombinant human collagen scaffold. *Biomaterials*, 35(8): 2420-2427.
https://doi.org/10.1016/j.biomaterials.2013.11.079

Gain P, Jullienne R, He ZG, et al., 2016. Global survey of corneal transplantation and eye banking. *JAMA Ophthalmol*, 134(2):167-173.
https://doi.org/10.1001/jamaophthalmol.2015.4776

Gill EL, Li X, Birch MA, et al., 2018. Multi-length scale bioprinting towards simulating microenvironmental cues. *Bio-Des Manuf*, 1(2):77-88.
https://doi.org/10.1007/s42242-018-0014-1

Gullstrand A, 1910. The optical system of the eye. *Physiol Opt*, 1:350-358.

Isaacson A, Swioklo S, Connon CJ, 2018. 3D bioprinting of a corneal stroma equivalent. *Exp Eye Res*, 173:188-193.
https://doi.org/10.1016/j.exer.2018.05.010

Kiely PM, Smith G, Carney LG, 1982. The mean shape of the human cornea. *Opt Acta: Int J Opt*, 29(8):1027-1040.
https://doi.org/10.1080/713820960

Kim H, Park MN, Kim J, et al., 2019. Characterization of cornea-specific bioink: high transparency, improved in vivo safety. *J Tissue Eng*, 10:1-12.
https://doi.org/10.1177/2041731418823382

Lawrence BD, Marchant JK, Pindrus MA, et al., 2009. Silk film biomaterials for cornea tissue engineering. *Biomaterials*, 30(7):1299-1308.
https://doi.org/10.1016/j.biomaterials.2008.11.018

Lawrence BD, Pan Z, Liu AH, et al., 2012. Human corneal limbal epithelial cell response to varying silk film geometric topography in vitro. *Acta Biomater*, 8(10):3732-3743.
https://doi.org/10.1016/j.actbio.2012.06.009

Levis HJ, Peh GSL, Toh KP, et al., 2012. Plastic compressed collagen as a novel carrier for expanded human corneal endothelial cells for transplantation. *PLoS ONE*, 7(11): e50993.
https://doi.org/10.1371/journal.pone.0050993

Meek KM, Knupp C, 2015. Corneal structure and transparency. *Prog Retin Eye Res*, 49:1-16.
https://doi.org/10.1016/j.preteyeres.2015.07.001

Mi SL, Chen B, Wright B, et al., 2010. *Ex vivo* construction of an artificial ocular surface by combination of corneal limbal epithelial cells and a compressed collagen scaffold containing keratocytes. *Tissue Eng Part A*, 16(6):2091-2100.
https://doi.org/10.1089/ten.tea.2009.0748

Na K, Shin S, Lee H, et al., 2018. Effect of solution viscosity on retardation of cell sedimentation in DLP 3D printing of gelatin methacrylate/silk fibroin bioink. *J Ind Eng Chem*, 61:340-347.
https://doi.org/10.1016/j.jiec.2017.12.032

Sasaki S, Funamoto S, Hashimoto Y, et al., 2009. In vivo evaluation of a novel scaffold for artificial corneas prepared by using ultrahigh hydrostatic pressure to decellularize porcine corneas. *Mol Vis*, 15:2022-2028.

Taylor ZD, Garritano J, Sung S, et al., 2015. THz and mm-wave sensing of corneal tissue water content: electromagnetic modeling and analysis. *IEEE Trans Terahertz Sci Technol*, 5(2):170-183.
https://doi.org/10.1109/TTHZ.2015.2392619

Torricelli AAM, Wilson SE, 2014. Cellular and extracellular matrix modulation of corneal stromal opacity. *Exp Eye Res*, 129:151-160.
https://doi.org/10.1016/j.exer.2014.09.013

Wang BH, Xu YS, Xie WJ, et al., 2018. Effects of corneal thickness distribution and apex position on postoperative refractive status after full-bed deep anterior lamellar keratoplasty. *J Zhejiang Univ-Sci B (Biomed & Biotechnol)*, 19(11):863-870.
https://doi.org/10.1631/jzus.B1800230

Ying GL, Jiang N, Yu CJ, et al., 2018. Three-dimensional bioprinting of gelatin methacryloyl (GelMA). *Bio-Des Manuf*, 1(4):215-224.
https://doi.org/10.1007/s42242-018-0028-8

Yoeruek E, Bayyoud T, Maurus C, et al., 2012. Decellularization of porcine corneas and repopulation with human corneal cells for tissue-engineered xenografts. *Acta Ophthalmol*, 90(2):e125-e131.
https://doi.org/10.1111/j.1755-3768.2011.02261.x

Zhang B, Gao L, Gu L, et al., 2017. High-resolution 3D bioprinting system for fabricating cell-laden hydrogel scaffolds with high cellular activities. *Procedia CIRP*, 65: 219-224.
https://doi.org/10.1016/j.procir.2017.04.017

Zhang B, Xue Q, Li JT, et al., 2019. 3D bioprinting for artificial cornea: challenges and perspectives. *Med Eng Phys*, 71: 68-78.
https://doi.org/10.1016/j.medengphy.2019.05.002

中文概要

题　目：集成式生物 3D 打印构建几何结构可控的角膜替代物方法

目　的：供体角膜短缺是一个全球性问题。现有的角膜替代物主要依赖于传统的组织工程制造方法，仅支持具有不可控曲率的平坦或弯曲膜的制备。我们提出构建具有设计几何特征的弯曲薄膜，以通过

生物 3D 打印实现厚度及曲率半径可控的角膜替代物。

创新点：提出一种集成的 3D 角膜替代物打印系统，为 3D 角膜支架提供了一种新颖的制作方法；提出角膜光学特性与角膜支架几何特征的关系，并分析影响角膜光学功能的相关影响因素。根据扫描数据，采用该方法可以快速构建具有天然角膜几何形状和尺度的角膜支架。使用该方法可获得具有高细胞活力的载有细胞的复杂弯曲角膜状结构。该方法具有低制造成本和高重复性，是根据需要快速构建角膜预替代物的有效方法。

方　法：通过建立角膜数学模型，研究维持角膜视功能和生理学的关键几何参数和其他主导因素；根据天然角膜的表面拓扑结构，通过计算机辅助设计对精确定制的人造角膜进行建模；通过集成数字光处理和挤出生物打印来制备用于角膜替代的曲面薄膜。

结　论：由于结构可控性等优点，生物 3D 打印是制备具有几何结构可控人工生物合成角膜的有效工具，可以个性化构建具有天然角膜尺度的角膜替代物。

关键词：生物 3D 打印；角膜替代物；光固化打印；挤出打印；结构控制